On Numerical Shock Thickness of Recently Proposed Euler Fluxes and SLAU2 in Hypersonic Flow Simulations

K. Kitamura* and Y. Shuto*
Corresponding author: kitamura@ynu.ac.jp

* Yokohama National University, Japan

Keywords: Numerical Algorithms; Computational Fluid Dynamics; Hypersonic Flow; Carbuncle Phenomena.

1 Introduction

The Simple Low-dissipation Advection-Upstream-splitting-method 2 (SLAU2) [1] is one of Euler fluxes used to compute the numerical flux at cell interfaces in the finite volume method (FVM). The SLAU2 was developed based on the numerical experiments conducted by Kitamura-Roe-Ismail [2], leading to a robust and accurate sequel to SLAU [3] for hypersonic flow computations. Many applications such as [4, 5] have been reported since the development of the SLAU2. Nevertheless, researchers have been trying to enhance, improve, or extend it [6, 7] and construct a new one in pursuit of more robust alternatives. This study will first compare their performance in our hypersonic flow numerical test [2], as well as the matrix stability analysis [23, 27, 28, 24]. Then, our discussions will be extended to the thickness of the numerically expressed shockwave by each method and their link to the robustness against shock anomalous solutions such as carbuncles [2, 8].

2 Numerical Experiment of 1.5D Normal Shock

2.1 Numerical Setup

The 2D compressible Euler equations are solved using the FVM with first-order accuracy in both time and space.

$$\frac{\partial \mathbf{u}}{\partial t}+\frac{\partial \mathbf{F}}{\partial x}+\frac{\partial \mathbf{G}}{\partial y}=0 \tag{1a}$$

$$\mathbf{u}=\begin{bmatrix}\rho\\ \rho u\\ \rho v\\ \rho e_t\end{bmatrix},\quad \mathbf{F}=\begin{bmatrix}\rho u\\ \rho u^2+p\\ \rho uv\\ \rho uH\end{bmatrix},\quad \mathbf{G}=\begin{bmatrix}\rho v\\ \rho vu\\ \rho v^2+p\\ \rho vH\end{bmatrix} \tag{1b}$$

here ρ is density, u and v velocity components in Cartesian coordinates, p pressure, e_t total energy, H total enthalpy ($H=e_t+p/\rho$). The calorically perfect gas model is assumed for air with the specific heat ratio γ =1.4. The numerical flux functions employed include recently proposed AUSM+M [9], AUSM2025p [10], and AUSM2025u [10], as well as SLAU2, AUSM+ [11], and Roe [12] with entropy-fix ('E-Fix') [13]. Formulations for selected flux functions are found in Appendix A.

Following [2], the computational domain was prepared as shown in Fig. 1. The computational grid comprises 50×25 cells evenly spaced without perturbations. A steady shock that includes an intermediate state is prescribed with initial conditions for left (L: i≤12) and right (R: i≥14) following the Rankine-Hugoniot conditions across the normal shock with the freestream Mach number M_0=6.0, 10.0, or 20.0. This problem is called the "1.5D (or 1-1/2-D) problem," which was conducted in Ref. [2] to examine the robustness of the flux functions in capturing a steady normal shock in a two-dimensional rectangular domain. This setup mimics a close-up view of a hypersonic flow ahead of the stagnation point of a two-dimensional blunt body; hence, it largely predicts the results of such flow computations. Readers are encouraged to refer to Ref. [2] for details. The internal shock conditions (M: i=13) are as follows.

1) The density is given as

$$\rho_M = \varepsilon \rho_L + (1 - \varepsilon)\, \rho_R \tag{2}$$

where the shock-position parameter ε = 0.0, 0.1, ... , 0.9 (following the notation in [2], which was denoted as 1-α_ρ in [23, 27]). The initial shock is imposed exactly on the cell interface when ε=0.0, and at the cell center when ε=0.5.

2) The other variables are calculated based on ρ_M, such that all variables lie on the Hugoniot curve [29]. No perturbations were introduced into the initial conditions.

3) The computations were conducted for 40,000 steps with CFL=0.5. We note that longer timesteps or a smaller CFL essentially did not affect the solutions. If a flux function is stable for all the shock positions of ε, the flux is regarded as robust as SLAU2, Van Leer's FVS [14], and HLLE [30].

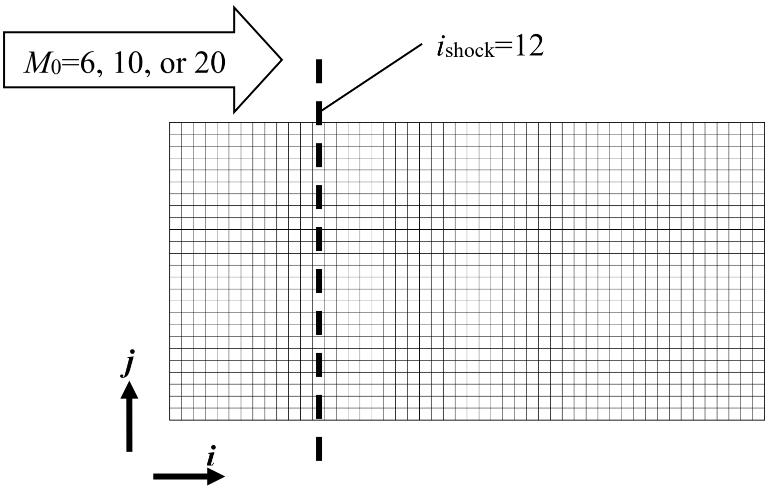

Figure 1: Computational Grid and Conditions for 1.5D Steady Shock Test Problem [2].

2.2 Numerical Results

Typical solutions are shown in Figs. 2 and 3 for Mach 6 and 20, respectively. Note that these solutions are largely similar and nearly insensitive to the upstream Mach numbers. This trend was already reported in literature [2, 23, 27], and thus, Mach 10 results are omitted here.

- '2' denotes a stable and symmetric solution with at least three orders of (L2-norm of) density residual reduction.
- '1' denotes an asymmetry and/or oscillation of the shock confined within three cells of the shock normal direction.
- '0' denotes an unstable solution usually associated with the total breakdown of the shock ("carbuncle"). The residual stagnated at a significant value.

All solutions based on these scores are listed in Table 1 for Mach 6 (but largely common to Mach 10 and 20).

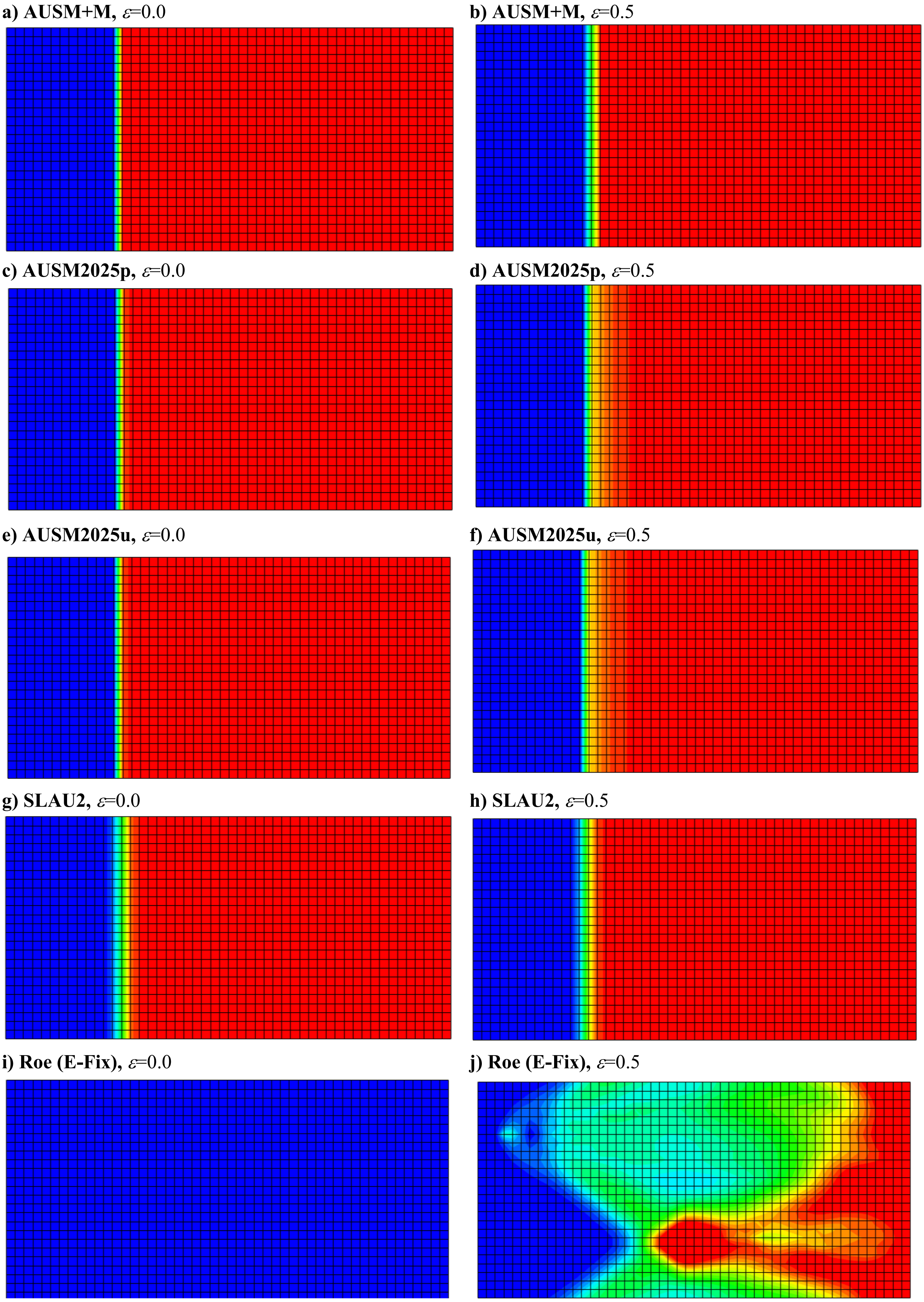

Figure 2: Computational Grid and Conditions for 1.5D Steady Shock Test Problem (M_0=6.0).

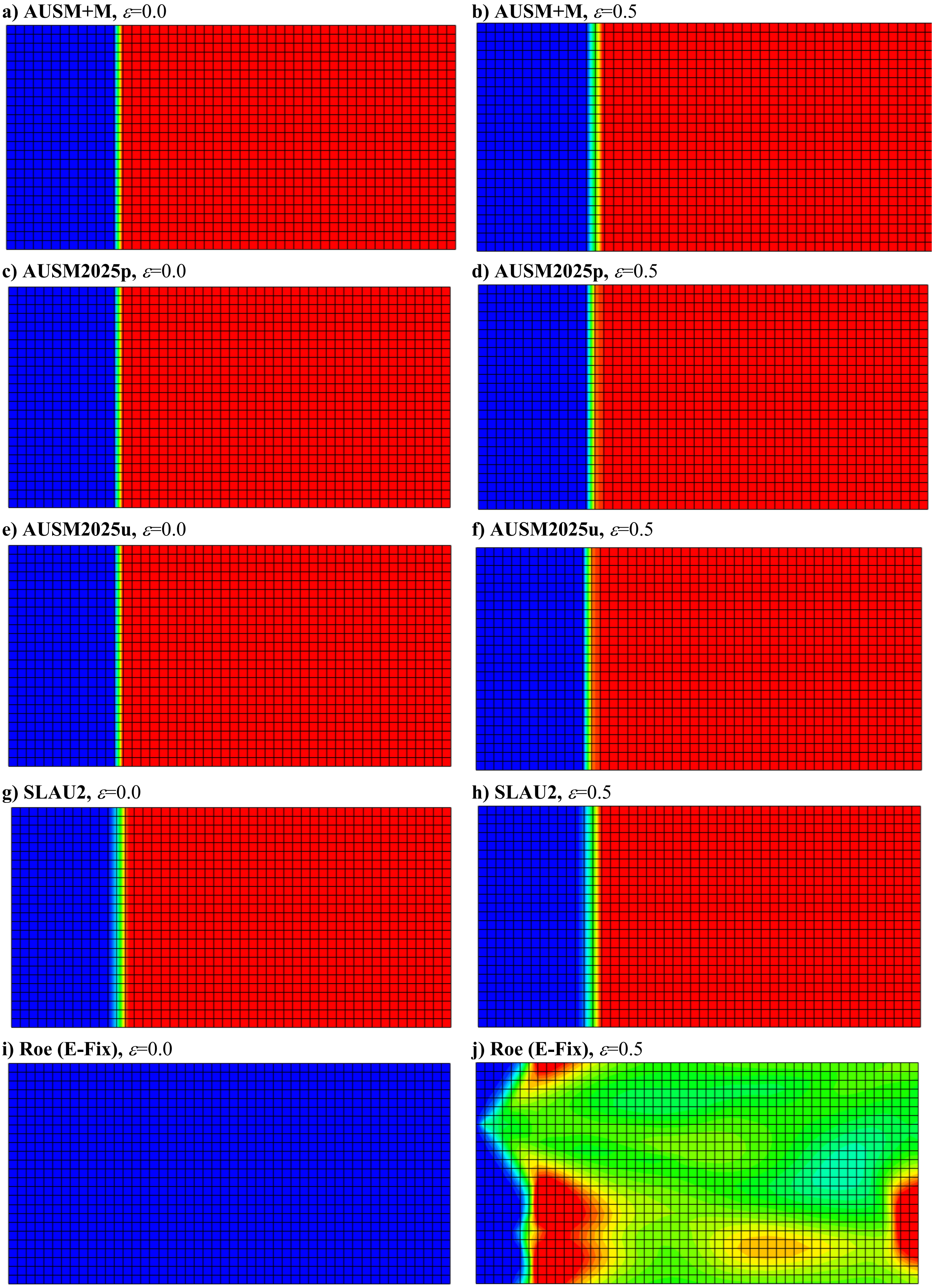

Figure 3: Computational Grid and Conditions for 1.5D Steady Shock Test Problem (M_0=20.0).

Table 1. 1.5D test results for various numerical flux functions (ε: shock location parameter [2]).

Numerical Flux Functions	ε=0.0	0.1	0.2	0.3	0.4	0.5	0.6	0.7	0.8	0.9	Total
AUSM+M [9]	**2**	**2**	**2**	**2**	**2**	**2**	**2**	**2**	**2**	**2**	**20**
AUSM2025p [10]	**2**	**2**	**2**	**2**	**2**	**2**	**2**	**2**	**2**	**2**	**20**
AUSM2025u [10]	**2**	**2**	**2**	**2**	**2**	**2**	**2**	**2**	**2**	**2**	**20**
SLAU2 [1]	**2**	**2**	**2**	**2**	**2**	**2**	**2**	**2**	**2**	**2**	**20**
AUSM+ [11]	**2**	**2**	**2**	**2**	1	1	1	1	**2**	**2**	16
Roe (E-Fix) [12, 13]	0	0	0	0	0	0	0	0	0	0	0

- All the tested, recently-proposed flux functions (AUSM+M*, AUSM2025p, and AUSM2025u) yielded stable and satisfactory solutions, in contrast with the classical AUSM+ and Roe (E-Fix). In particular, Roe (E-Fix) showed the total breakdown of the shock, leading to the carbuncle solutions.
- The numerical shock thickness is wider (spanning over two cells – 'mild') for the ε = 0.5 setup than for ε = 0.0 (confined with one cell – 'sharp') in the newer three methods (AUSM+M, AUSM2025p, and AUSM2025u), depending on the initial shock setup. In contrast, the shock stays thick (over two to three cells – 'thick') in SLAU2 solutions, regardless of its initial location. This is consistent with the development philosophy of the SLAU2, in which the shock thickness is allowed to be expressed by a few cells.

The second aspect is important and interesting, because it tells us that there exist shock-stable solvers categorized into two, i.e.,

1) 'Thin' Shock Capturing Methods: AUSM+M, AUSM2025p, and AUSM2025u try to capture the shock as thin as possible together with additional dissipation term(s).
2) 'Thick' Shock Capturing Methods: SLAU2 intentionally expresses the shock broadly which successfully stabilized the solution. Van Leer and HLLE may also fall into this category, although they, as opposed to SLAU2, are known to fail in expressing boundary-layers economically [16].

In the next section, we will test these fluxes in the widely-used matrix linear stability analysis [23, 27], and try to relate the results of the analysis with the thickness of a numerically captured shockwave for each flux function.

Before moving on to Sec. 3, we would like to mention that according to the numerical solutions, Methods 1) and 2) behaved similarly, regardless of the thickness of the captured shockwaves. We would like to emphasize also that 2) SLAU2, while broadening the captured shock, reportedly showed satisfactory hypersonic heating prediction capabilities in [1], demonstrating its excellent total enthalpy conservation across the shock and the thermal boundary-layer resolution in proximity to the wall [16].

3 Matrix Stability Analysis

The matrix stability analysis [23, 27] has been widely used in the analysis of numerical flux functions for evaluating their performance at captured shocks. In this linear analysis, we assume

$$\bar{Q}_i = \hat{Q}_i + \delta\bar{Q}_i \tag{3}$$

where $\hat{Q}_i$ is the steady mean value and $\delta\bar{Q}_i$ is the small perturbation. Substituting (3) into the governing equation (compressible Euler equations), Eq.(1), and linearizing the numerical flux function, we obtain the perturbation evolution of all $q = \mathrm{N} \cdot \mathrm{M}$ cells in the domain consisting of N (=11) rows and M (=11) columns,

* There was a confusion while one of the authors read the original paper [9] for formulating AUSM+M, particularly in its "p_{uy}" term [Eq.(A.34)]. As a result, this term was *not* included in our 2D code, in which momentum equations are written in cell-interface-normal (where only "p_{ux}" is included) and cell-interface-tangential directions.

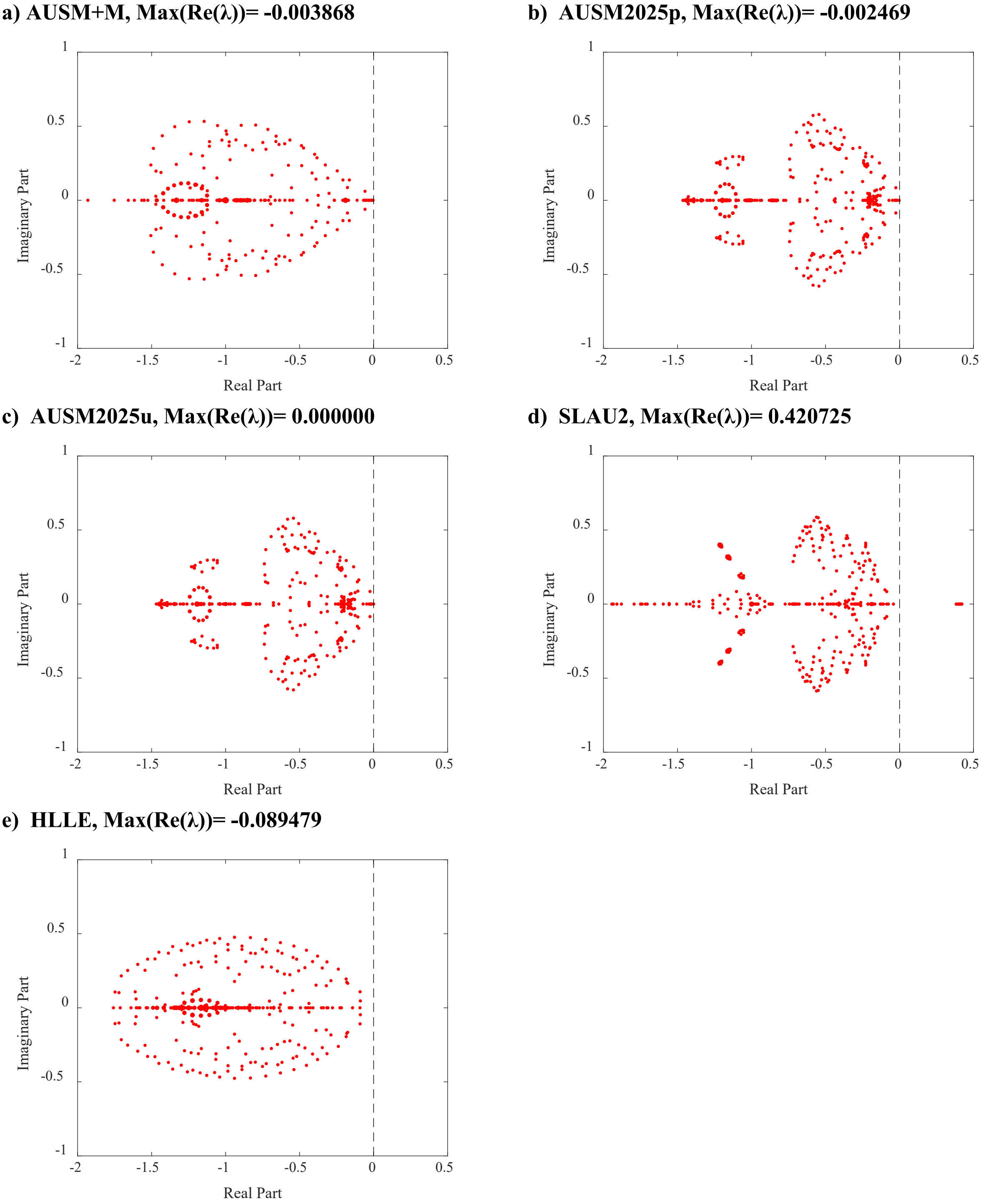

Figure 4: Matrix Stability Analysis of Recently-Proposed Methods (M_0=6, α_ρ=0.0).

$$\frac{d}{dt}\begin{pmatrix}\delta\overline{Q}_1\\ \vdots\\ \delta\overline{Q}_q\end{pmatrix} = S\begin{pmatrix}\delta\overline{Q}_1\\ \vdots\\ \delta\overline{Q}_q\end{pmatrix} \tag{4}$$

where S is the stability matrix. The perturbation remains bounded if the maximum of the real part of the eigenvalue λ of S is non-positive,

$$\max(\mathrm{Re}(\lambda)) \le 0 \tag{5}$$

The flux Jacobian in S is evaluated numerically using a centered approximation as proposed in [23], in order to handle the non-differentiability of numerical flux functions (as conducted for ideal MHD [24]). Random numerical perturbations of the order 10^{-6} are introduced into the entire flow field to trigger instabilities [24]. The details are found in [23]. The upstream Mach number is set as $M_0 = 6.0$, corresponding to the baseline numerical text in the previous section.

3.1 Results for $\alpha_\rho = 0$

The first analysis assumes that the shock has 'no thickness' ($\alpha_\rho = 1 - \varepsilon = 0$ in Eq.(2)), and the results for 1) AUSM+M, AUSM2025p, and AUSM2025u and 2) SLAU2 are shown in Figs. 4, including HLLE for a comparison purpose. It has been demonstrated that 1) AUSM+M, AUSM2025p, and AUSM2025u satisfy Eq. (5), whereas 2) SLAU2 does not. Thus, while the results of this stability analysis for Methods 1) *support the solutions of numerical experiment*, those for 2) SLAU2 *contradict with it*. This will be explained in the next subsection, and more detailed mode breakdowns will appear in Appendix B.

3.2 Results for $\alpha_\rho = 0, 0.1, \ldots, 1.0$

Then, let us parametrize α_ρ next. If the initial shock is located somewhere within the shock, its relative location to the gridline is denoted as $\alpha_\rho = 1\text{-}\varepsilon$ in Eq.(2). The results for varied α_ρ are summarized in Fig. 5 and Table 2. It is discovered that any of 1) AUSM+M, AUSM2025p, and AUSM2025u and 2) SLAU2 violate Eq.(5) for certain initial locations α_ρ. Specifically, AUSM2025p and AUSM2025u showed peaky profiles at $\alpha_\rho = 0.4$ (followed by $\alpha_\rho = 0.5$), reaching large values between 4 and 5 of $\max(\mathrm{Re}(\lambda))$. This indicates a potential risk of instability, although not confirmed from the corresponding numerical experiments (Figs. 2 and 3). This difference between the numerical solution (Table 1) and the stability analysis (Table 2) at $\alpha_\rho = 0.4$ and 0.5 could be explained as follows: i) The matrix stability analysis predicts the numerical response of the selected flux function to the initial shock locations α_ρ ; ii) In the numerical simulations, however, the shock can spread over at least one cell, particularly when the initial shock was away from the grid line ($\alpha_\rho \neq 0$); iii) Eventually, the shock can reside at a different position from the initial one. In this scenario, the matrix analysis cannot accurately predict the shock stability due to this displacement. While the matrix analysis is still useful in assessing the shock stability of a flux function, this important aspect was not

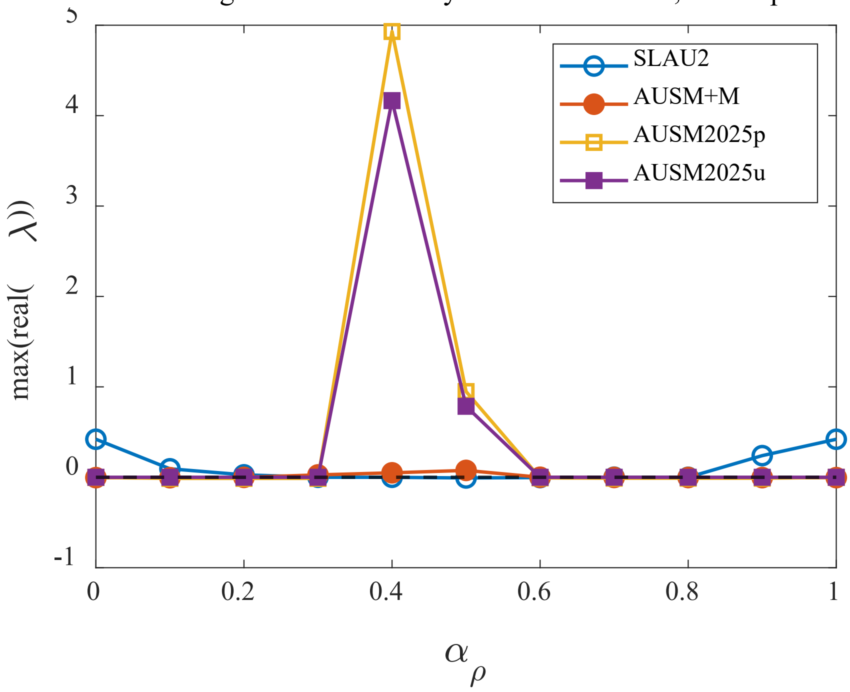

Figure 5: Matrix Stability Analysis Results of Recently-Proposed Methods and SLAU2 for varied Shock Locations α_ρ (M_0=6).

reported in literature, to the best of the authors' knowledge.

AUSM+M, on the other hand, showed a nearly flat profile against α_ρ, exhibiting 0.076 as the maximum value for $\max(\mathrm{Re}(\lambda))$ at α_ρ = 0.5. But again, this does not mean that the numerical solution is unstable, as confirmed from Table 1. In terms of the fluctuations of $\max(\mathrm{Re}(\lambda))$, SLAU2 behaved similarly, although it showed positive $\max(\mathrm{Re}(\lambda))$ at α_ρ = 0.0 and negative value at α_ρ = 0.5 (nearly opposite to AUSM+M).

We would like to point out that it is generally difficult to avoid a specific shock location α_ρ (such as 0.4 or 0.5) in practice. This is because in many shock-capturing flow simulations (in particular, shock-shock and/or shock-boundary-layer interactions [21, 22]), the shockwave locations cannot be predicted *a priori*, nor be the computational grid prepared to fit them. Furthermore, moving shockwaves experience all the locations α_ρ [17, 18]. Therefore, it would be reasonable to select or construct a flux function which behaves robustly against the shock at all possible locations α_ρ, which should be *confirmed not only from the matrix analysis but from numerical tests*.

Table 2: Matrix Stability Analysis Results Summary for varied Shock Locations α_ρ (M_0=6).

α_ρ	SLAU2	AUSM+M	AUSM2025p	AUSM2025u
0.0	0.420725	-0.00387	-0.002469	0
0.1	0.093854	-0.00458	-0.012261	0
0.2	0.027215	-0.00103	-0.012369	0
0.3	0.0001	0.026371	-0.012401	0
0.4	-0.0001	0.049367	4.930244	4.166067
0.5	-0.00751	0.076086	0.948144	0.785198
0.6	-0.003098	0.000113	-0.006683	0
0.7	0.001054	-0.00173	-0.010263	0
0.8	-0.0001	-0.00246	-0.010345	0
0.9	0.239566	-0.00367	-0.010458	0
1.0	0.420591	-0.00383	-0.001088	0

4 Concluding Remarks

It has been numerically demonstrated that the recently proposed Euler fluxes, i.e., AUSM+M [9], AUSM2025p [10], and AUSM2025u [10], are as robust as SLAU2 against the notorious carbuncle phenomena or other shock-related anomalous solutions, despite numerically represented shockwaves being thinner. Then, we conducted a matrix linear stability analysis for each of the numerical fluxes.

According to the matrix analysis, while useful and widely used for assessing the numerical robustness of a flux function against the 'thin' shock, it is found to be unable to universally predict the performance of the selected method, particularly when the shock is 'thickened' as the time evolves. This important aspect has long been largely ignored in the community.

In this respect, Ida et al. [26] argued the numerical and theoretical expressions for the shock thickness of SLAU2. However, as indicated in this work, the SLAU2 (Method 2) behaves somewhat differently from the other fluxes (Methods 1), and hence, their universality is questionable.

Nevertheless, according to literature and our own experiences, all these successful fluxes still have the potential to provoke carbuncles in more challenging setups (e.g., with higher cell aspect ratios [15, 16] or moving shock waves [17, 18]). Furthermore, it is unclear whether these methods economically resolve contact discontinuities and boundary-layers, which are crucial for aeroheating predictions in hypersonic flows [19, 20, 21]. These will also be surveyed near future.

The future work will also cover other flux functions, such as LDFSS2025u/p/M [10] and AUSMDV2+ [25]. These will strongly contribute to further understanding and development of numerical flux functions. Moving shock tests [17, 18], in which the shock experiences any possible locations relative to the gridlines, will hopefully provide some clues. Apart from this, a shock/shock or shock/boundary-layer interaction examples [21, 22] are also of importance from an engineering application point of view.

Acknowledgements

This work was supported by JSPS KAKENHI Grant Number JP26K01133.

References

[1] K. Kitamura and E. Shima. J. Comput. Phys., 245:62-83, 2013.
[2] K. Kitamura, P. Roe, and F. Ismail. AIAA J., 47:44-53, 2009.
[3] E. Shima and K. Kitamura. AIAA J., 49:1693-1709, 2011.
[4] E. Molina, B.Y., Zhou, J.J., Alonso, M., Righi and R.G. Silva. AIAA 2019-0326, 2019.
[5] G. Wilke, J. Bailly, K. Kimura, and Y. Tanabe. CEAS Aeronaut. J., 13:313–333, 2022.
[6] J. Aono and K. Kitamura. J. Comput. Phys., 462: 111256, 2022.
[7] T. Mamashita, K, Kitamura, K., and T. Minoshima. Comp. Fluids, 231: 105165, 2021.
[8] M. Pandolfi, and D. D'Ambrosio. J. Comput. Phys., 166:271-301, 2001.
[9] S.-S. Chen, F.-J. Cai, H.-C. Xue, N. Wang, and C. Yan. Applied Math. Modeling, 77:1065-1081, 2020.
[10] A.K. Pandare and J.R. Edwards. J. Comput. Phys., 543: 114415, 2025.
[11] M.-S. Liou. J. Comput. Phys., 129:364-382, 1996.
[12] P.L. Roe. J. Comput. Phys., 43:357-372, 1981.
[13] A. Harten. J. Comput. Phys., 49:357-393, 1983.
[14] B. Van Leer. ICASE Rept. 82-30, 1982.
[15] S.J. Henderson and J.A. Menart. AIAA 2007-3904, 2007.
[16] K. Kitamura, E. Shima, Y. Nakamura, and P.L. Roe. AIAA J., 48:763-776, 2010.
[17] J.J. Quirk. Int. J. Numer. Meth. Fluids, 18:555-574, 1994.
[18] K. Kitamura and E. Shima. AIAA J., 57:1763-1772, 2019.
[19] A. Knutson, C. Switala, T. Drayna, P. Subbareddy, and G.V. Candler. AIAA 2026-1722, 2026
[20] P.A. Gnoffo, AIAA Paper 2009-599, 2009.
[21] A.R. Wieting and M.S. Holden. AIAA J., 27:1557-1565, 1989.
[22] B. Edney, FFA Rept. 115, 1968.
[23] M. Dumbser, J.M. Moschetta, and J. Gressier. J. Comput. Phys., 197: 647-670, 2004.
[24] Y. Shuto and K. Kitamura, ICCFD13, 2026.
[25] S. Phongthanapanich and A. Matthujak. Shock Waves, 31:901-927, 2021.
[26] R. Ida, Y. Tamaki, and S. Kawai. J. Comput. Phys., 505: 2901, 2024.
[27] Y. Chauvat, J.-M. Moschetta, and J. Gressier. Int. J. Numer. Meth. Fluids, 47: 903-909, 2005.
[28] L. Hu, and Z. Feng. Comm. Nonlin. Sci. Numer. Sim., 116: 106798, 2023.
[29] T. J. Barth. NASA TM-101087, 1989.
[30] A. Harten, P. Lax, and B. van Leer. SIAM Rev., 25: 35-61, 1983.
[31] K.H. Kim, C. Kim, O.H. Rho. J. Comput. Phys., 174: 38-80, 2001.

Appendix A: Numerical Flux Functions

A.1 AUSM+ [11]

$$\mathbf{F}_{1/2(AUSM+)} = \frac{\dot{m}_{1/2} + \left|\dot{m}_{1/2}\right|}{2}\mathbf{\Psi}_L + \frac{\dot{m}_{1/2} - \left|\dot{m}_{1/2}\right|}{2}\mathbf{\Psi}_R + \mathbf{P} \tag{A.1}$$

$$\mathbf{\Psi} = (1, u, v, H)^T, \quad \mathbf{P} = (0, p_{1/2}, 0, 0)^T \tag{A.2}$$

$$\dot{m}_{1/2} = \rho_L a_{1/2} \max(0, M_{1/2}) + \rho_R a_{1/2} \min(0, M_{1/2}) \tag{A.3}$$

$$M_{1/2} = \mathrm{M}^+ + \mathrm{M}^- \tag{A.4}$$

$$p_{1/2} = \mathrm{P}^+ \cdot p_L + \mathrm{P}^- \cdot p_R \tag{A.5}$$

$$a_{1/2} = \min(\tilde{a}_L, \tilde{a}_R), \quad \tilde{a} = a^{*2} / \max(a^*, |u|) \tag{A.6}$$

$$\mathrm{M}^\pm = \begin{cases} \frac{1}{2}(M \pm |M|), & if\ |M| \geq 1 \\ \pm\frac{1}{4}(M \pm 1)^2 \pm \beta(M^2 - 1)^2, & otherwise \end{cases} \tag{A.7}$$

$$\mathrm{P}^\pm = \begin{cases} \frac{1}{2}(1 \pm sign(M)), & if\ |M| \geq 1 \\ \frac{1}{4}(M \pm 1)^2(2 \mp M) \pm \alpha M(M^2 - 1)^2, & otherwise \end{cases} \tag{A.8}$$

where $\alpha = 3/16$, $\beta = 1/8$ are recommended, and

$$a^{*2} = \frac{2(\gamma - 1)}{(\gamma + 1)} H \tag{A.9}$$

is the critical speed of sound.

A.2 AUSMPW+ [31]

They replaced the numerical speed of sound with the following one.

$$a_{1/2} = \begin{cases} \dfrac{a_s^2}{\max(|u_L|, a_s)} & if \quad \frac{1}{2}(u_L + u_R) > 0 \\ \dfrac{a_s^2}{\max(|u_R|, a_s)} & if \quad \frac{1}{2}(u_L + u_R) < 0 \end{cases} \tag{A.10}$$

$$a_s^2 = \frac{2(\gamma - 1)}{(\gamma + 1)} H_{normal} \tag{A.11}$$

$$H_{normal} = \frac{1}{2}\left(H_L - \frac{v_L^2}{2} + H_R - \frac{v_R^2}{2}\right) \tag{A.12}$$

where H_{normal} is the total enthalpy H excluding the shock-tangential velocity contribution, v_L and v_R. Other terms in this method is omitted here.

A.3 SLAU (Simple Low-dissipation AUSM) [3]

$$\boldsymbol{F}_{SLAU} = \frac{\dot{m} + |\dot{m}|}{2}\boldsymbol{\Psi}^{+} + \frac{\dot{m} - |\dot{m}|}{2}\boldsymbol{\Psi}^{-} + \mathbf{P} \tag{A.13}$$

$$\boldsymbol{\Psi} = (1,\ u,\ v,\ H)^T, \quad \mathbf{P} = \left(0,\ p_{1/2},\ 0,\ 0\right)^T \tag{A.14}$$

and the mass flux is given by

$$(\dot{m})_{SLAU} = \frac{1}{2}\left\{\rho_L(u_L + |\bar{V}_n|^{+}) + \rho_R(u_R - |\bar{V}_n|^{-}) - \frac{\chi}{a_{1/2}}\Delta p\right\} \tag{A.15}$$

$$|\bar{V}_n|^{+} = (1-g)|\bar{V}_n| + g|u_L|, \quad |\bar{V}_n|^{-} = (1-g)|\bar{V}_n| + g|u_R| \tag{A.16}$$

$$|\bar{V}_n| = \frac{\rho_L|u_L| + \rho_R|u_R|}{\rho_L + \rho_R} \tag{A.17}$$

$$g = -\max[\min(M_L, 0), -1] \cdot \min[\max(M_R, 0), 1] \quad \in [0, 1] \tag{A.18}$$

where

$$\chi = (1-\widehat{M})^2 \tag{A.19}$$

$$\hat{M} = min\left(1.0, \frac{1}{a_{1/2}}\sqrt{\frac{\boldsymbol{u}_L{}^2 + \boldsymbol{u}_R{}^2}{2}}\right) \tag{A.20}$$

$$M = \frac{u}{a_{1/2}} \tag{A.21}$$

$$a_{1/2} = \bar{a} = \frac{a_L + a_R}{2} \tag{A.22}$$

Then, the pressure flux is

$$\begin{aligned} &p_{1/2(SLAU)} \\ &= \frac{p_L + p_R}{2} + \frac{\mathrm{P}^{+}|_{\alpha=0} - \mathrm{P}^{-}|_{\alpha=0}}{2}(p_L - p_R) \\ &+ (1-\chi)(\mathrm{P}^{+}|_{\alpha=0} + \mathrm{P}^{-}|_{\alpha=0} - 1)\frac{p_L + p_R}{2} \end{aligned} \tag{A.23}$$

$$\mathrm{P}^{\pm}\Big|_{\alpha} = \begin{cases} \frac{1}{2}(1 \pm sign(M)), & if\ |M| \geq 1 \\ \frac{1}{4}(M \pm 1)^2(2 \mp M) \pm \alpha M(M^2 - 1)^2, & otherwise \end{cases} \tag{A.24}$$

A.4 SLAU2 [1]

The dissipation term of the pressure flux has been modified from SLAU as

$$p_{1/2(SLAU2)} = \frac{p_L + p_R}{2} + \frac{P^+|_{\alpha=0} - P^-|_{\alpha=0}}{2}(p_L - p_R) + \sqrt{\frac{\boldsymbol{u}_L{}^2 + \boldsymbol{u}_R{}^2}{2}} \cdot (P^+|_{\alpha=0} + P^-|_{\alpha=0} - 1)\bar{\rho} a_{1/2} \tag{A.25}$$

$$\bar{\rho} = \frac{\rho_L + \rho_R}{2} \tag{A.26}$$

A.5 AUSM+M [9]

This method was constructed from AUSM+ ($\alpha = 3/16$) [11], with the speed of sound borrowed from AUSMPW+ [31].

$$\boldsymbol{F}_{AUSM+M} = \frac{\dot{m} + |\dot{m}|}{2}\boldsymbol{\Psi}^+ + \frac{\dot{m} - |\dot{m}|}{2}\boldsymbol{\Psi}^- + \mathbf{P} \tag{A.27}$$

$$\boldsymbol{\Psi} = (1,\ u,\ v,\ H)^T, \quad \mathbf{P} = \left(0,\ p_{1/2} \cdot n_x + p_{ux},\ p_{1/2} \cdot n_y + p_{uy},\ 0\right)^T \tag{A.28}$$

where in our locally 1D code, $n_x = 1$ and $n_y = 0$.

The other changes from AUSM+ lie in the mass flux and pressure fluxes. The mass flux is

$$M_{1/2(AUSM+M)} = M^+ + M^- + M_p \tag{A.29}$$

$$M_p = -\frac{1}{2}(1 - f) \cdot \frac{p_R - p_L}{\rho_{1/2} a_{1/2}^2} \cdot (1 - g) \tag{A.30}$$

$$f = \frac{1 - cos(\pi M)}{2}, M = min\left(1.0, max(|M_L|, |M_R|)\right) \tag{A.31}$$

$$g = \frac{1 + cos(\pi h)}{2}, h = min(h_k), h_k = min\left(\frac{p_{Lk}}{p_{Rk}}, \frac{p_{Rk}}{p_{Lk}}\right) \tag{A.32}$$

where k covers all the surrounding cells of both cells L and R.

The pressure flux has a similar form to that of SLAU, i.e.,

$$p_{1/2(AUSM+M)} = \frac{p_L + p_R}{2} + \frac{\mathrm{P}^+|_{\alpha=0} - \mathrm{P}^-|_{\alpha=0}}{2}(p_L - p_R) + f_0 \cdot (\mathrm{P}^+|_{\alpha=0} + \mathrm{P}^-|_{\alpha=0} - 1)\frac{p_L + p_R}{2} \tag{A.33}$$

$$p_{ux} = -g \cdot \frac{\gamma(p_L + p_R)}{2a_{1/2}} \mathrm{P}^+|_{\alpha=0} \mathrm{P}^-|_{\alpha=0} (u_R - u_L),$$
$$p_{uy} = -g \cdot \frac{\gamma(p_L + p_R)}{2a_{1/2}} \mathrm{P}^+|_{\alpha=0} \mathrm{P}^-|_{\alpha=0} (v_R - v_L) \tag{A.34}$$

where f_0 = 1 in our super/hypersonic study.

Appendix B: Variable Breakdowns of Matrix Stability Analysis

Breakdowns of variables for the matrix stability analysis (Fig. 4) are given in Fig. A for more detailed discussions. AUSM+M, AUSM2025p and AUSM2025u exhibit 'sawtooth-like form' reported in [23] for Roe flux. Nevertheless, since signs of density ('rho') and energy ('energy') are common for 1) AUSM+M, AUSM2025p, and AUSM2025u, they are considered stable (and indeed satisfies Eq.(5)), which *supports the solutions of numerical experiment*. On the other hand, 2) SLAU2 exhibit both positive and negative modes, indicating unstable behavior from this matrix stability analysis, which *contradicts with the numerical experiment*. For reference, HLLE showed clean distributions which also satisfies Eq.(5).

a) AUSM+M, Max(Re(λ))= -0.003868

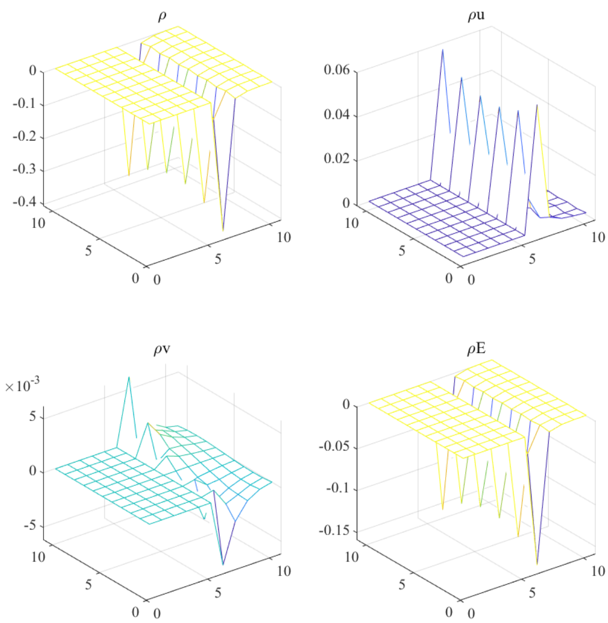

Figure A: Matrix Stability Analysis of Recently-Proposed Methods and SLAU2 (M_0 =6, α_ρ =0.0): Perturbation Distributions (Continued).

b) AUSM2025p, Max(Re(λ))= -0.002469

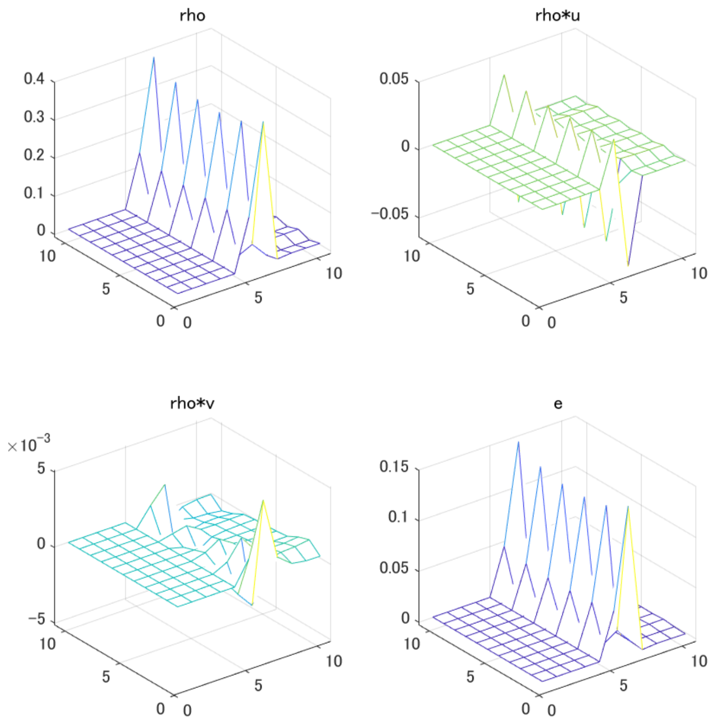

c) AUSM2025u, Max(Re(λ))= 0.000000

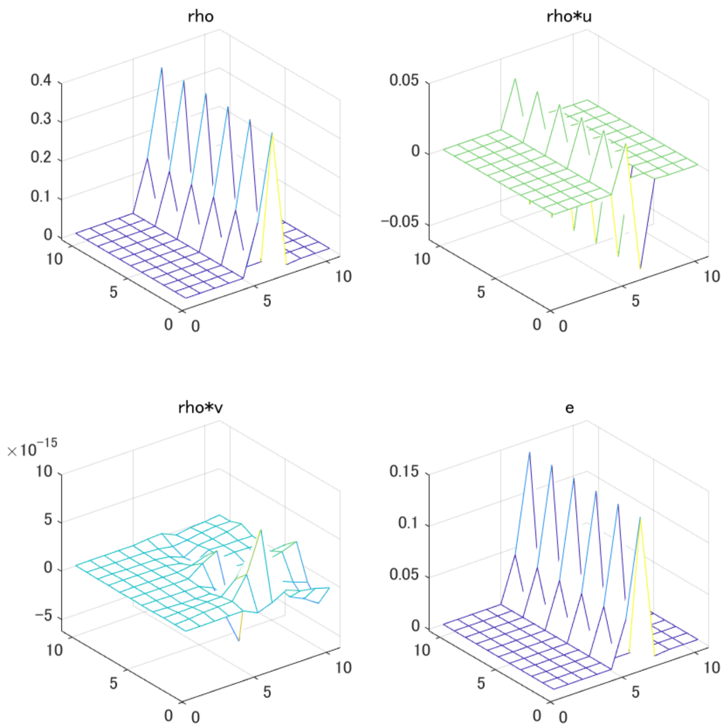

Figure A: Matrix Stability Analysis of Recently-Proposed Methods and SLAU2 (M_0=6, α_ρ =0.0): Perturbation Distributions (Continued).

d) SLAU2, Max(Re(λ))= 0.420725

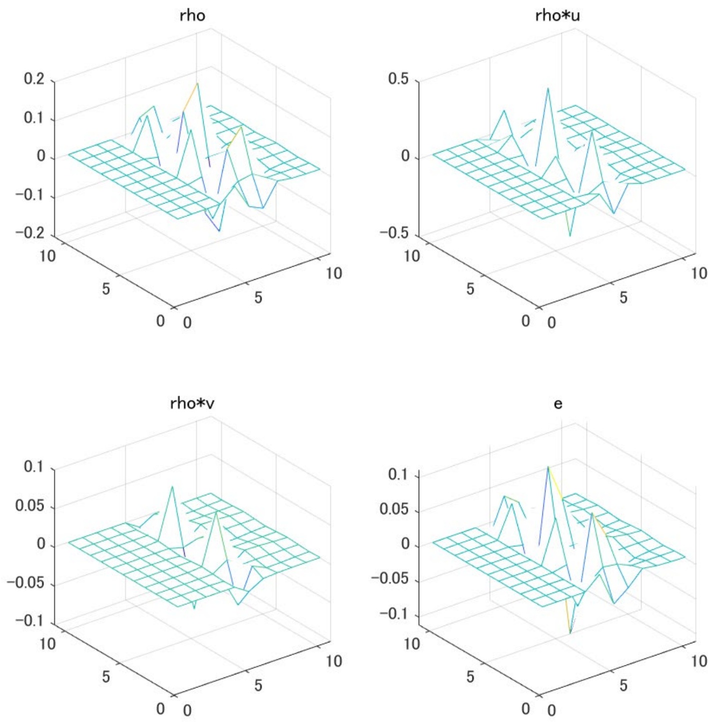

e) HLLE, Max(Re(λ))= -0.089479

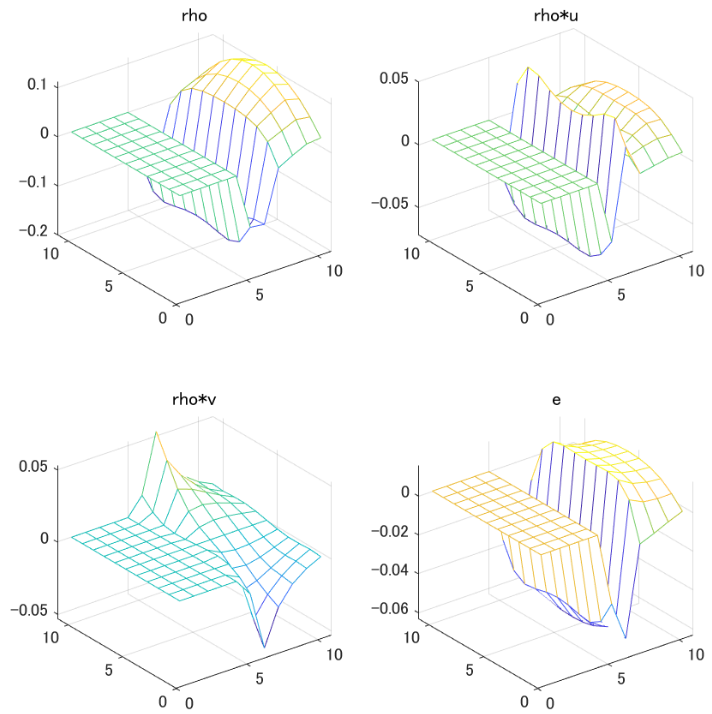

Figure A: Matrix Stability Analysis of Recently-Proposed Methods and SLAU2 (M_0=6, α_ρ=0.0): Perturbation Distributions (Concluded).